Link between lipid remodeling and ESCRT-III function in multivesicular body formation

Ralf Kölling[1]

Institut für Lebensmittelwissenschaft und Biotechnologie, Fg. Hefegenetik und Gärungstechnologie, Universität Hohenheim, 70599 Stuttgart, Germany

ralf.koelling@uni-hohenheim.de

[1]Corresponding author

Summary

It is still unclear how ESCRT-III acts on membranes. Here evidence is presented that ESCRT-III recruits a scramblase to the site of intraluminal vesicle formation at late endosomes indicating that a change in membrane composition is crucial for MVB formation.

Abstract

Despite a tremendous amount of work, it is still unclear how the endosomal sorting complex required for transport (ESCRT)-III complex acts in membrane remodeling and abscission. Here we present evidence that a change in membrane composition is connected to ESCRT-III function during multivesicular body (MVB) formation. The central observation was a strong synergistic effect of two mutations on the turnover of an endocytic cargo protein. One mutation deletes Tms1, a yeast SERINC homologue. Human SERINC3 and SERINC5 are HIV-1 restriction factors and have been shown to act as scramblases, flipping phospholipids between membrane leaflets. The other mutation deletes the Vps68 subunit of the Vps55/Vps68 complex, which loosely resembles Tms1 in its overall structure. The strong synergistic effect suggests that Tms1 and Vps55/Vps68 perform a similar function. Since we could also show that Vps55 physically interacts with ESCRT-III, we propose that a scramblase is recruited to ESCRT-III and prepares the membrane for intraluminal vesicles formation at MVBs.

Introduction

The endosomal sorting complex required for transport (ESCRT)-III complex is involved in a plethora of membrane remodeling processes in eukaryotic cells. Despite a tremendous and impressive amount of work, it is still unclear how exactly ESCRT-III performs its function (Gatta and Carlton, 2019; Henne et al., 2013; Pfitzner et al., 2021; Remec Pavlin and Hurley, 2020; Vietri et al., 2020). There are eight basic types of ESCRT-III proteins with some isoforms in higher eukaryotic cells; four of these (Snf7, Vps2, Vps20 and Vps24 in yeast) are considered to constitute ESCRT-III (Babst et al., 2002). The other members of this protein family are called ESCRT-III associated or ESCRT-III like (Azmi et al., 2008; Nickerson et al., 2006; Rue et al., 2008). The favored view is that ESCRT-III proteins form spiraling filaments on membrane surfaces

that in conjunction with the AAA-ATPase Vps4 exert mechanical force onto the membranes, which lead to their deformation and to scission events.

We have been especially interested in the ESCRT-III associated protein Mos10 (also known as Vps60) (Kranz et al., 2001). Recent evidence suggests that Mos10 forms an alternative ESCRT-III complex independent of the canonical Snf7 containing complex (Alsleben and Kölling, 2022; Pfitzner et al., 2023). Both complexes appear to be involved in the formation of intraluminal vesicles (ILVs) during multivesicular body (MVB) formation in the endocytic pathway (Pfitzner et al., 2023).

Recently, we identified Vps68 as an interaction partner of Mos10 (Alsleben and Kölling, 2022). Vps68 forms a complex with Vps55, whose role in endocytic trafficking has been studied previously (Belgareh-Touze et al., 2002; Huh et al., 2003; Schluter et al., 2008; Suzuki et al., 2021). Both proteins have a similar structure basically consisting of four transmembrane spanning segments (TMDs). Deletion of *VPS55* and/or *VPS68* has only a moderate effect on the degradation of endocytic cargo proteins (Alsleben and Kölling, 2022; Schluter et al., 2008). But here, we identified another factor (*TMS1*), whose deletion leads to a complete block in the degradation of an endocytic cargo protein in combination with the *VPS68* deletion. This strong synergistic effect suggests that the Vps55/Vps68 complex and Tms1 perform a similar function.

Tms1 is a yeast member of the SERINC (serine incorporator) protein family, a group of highly conserved membrane proteins with ten membrane spanning segments (Leonhardt et al., 2023; Pye et al., 2020). In humans there are five members of this protein family, SERINC1-5. Yeast Tms1 shows a remarkably high sequence identity of 33 % with human SERINC1. This high degree of conservation suggests that SERINCs perform a central function in eukaryotic cells. Initially it was thought that SERINC facilitates the incorporation of serine into phosphatidylserine and sphingolipids (Inuzuka et al., 2005), but in a later study no significant effect of SERINC expression on the lipid composition of producer cells could be detected, arguing against the initially proposed function (Trautz et al., 2017). SERINC3 and SERINC5 are HIV-1 restriction factors (Rosa et al., 2015; Usami et al., 2015). The presence of these proteins in the envelope of viral particles reduce HIV-1 infectivity by up to 100-fold. Normally, the HIV-1 Nef protein prevents the incorporation of SERINCs into viral particles by triggering their endocytosis. Recently, convincing evidence has been presented that SERINCs are scramblases (Leonhardt et al., 2023), non-ATP dependent lipid transporters, which flip phospholipids between the leaflets of the lipid bilayer.

Cryo-EM structures of human SERINC3 and SERINC5 and its *Drosophila* orthologue have been presented (Leonhardt et al., 2023; Pye et al., 2020). The ten TMDs of SERINC5 are arranged into two α-helical bundles consisting of four TMDs each, which are connected by an asymmetric cross of two TMDs. Vps55 and Vps68 consist of four TMDs each. Thus, it is conceivable that Vps55/Vps68 could be a distant, fragmented member of the SERINC family. There are no obvious sequence identities between Vps55/Vps68 and Tms1, but a relatedness may be difficult to prove. This is exemplified by Ice2, which was recently identified as another

SERINC member in yeast, only after extensive application of sophisticated bioinformatic tools (Alli-Balogun and Levine, 2021).

Our study establishes a link between lipid remodeling and ESCRT-III function. We show that the putative scramblase Vps55/Vps68 directly associates with ESCRT-III. An alteration of the lipid composition at the incipient budding site could be a precondition for the ESCRT-III dependent formation of an intraluminal vesicle. A crucial role of lipids in MVB formation has been pointed out before (Matsuo et al., 2004).

Results and discussion

Vps55 interacts with ESCRT-III

In our previous study we identified Vps68 as an interaction partner of ESCRT-III (Alsleben and Kölling, 2022). Since Vps68 forms a complex with Vps55 (Schluter et al., 2008), we were interested to see, if Vps55 as well associates with ESCRT-III.

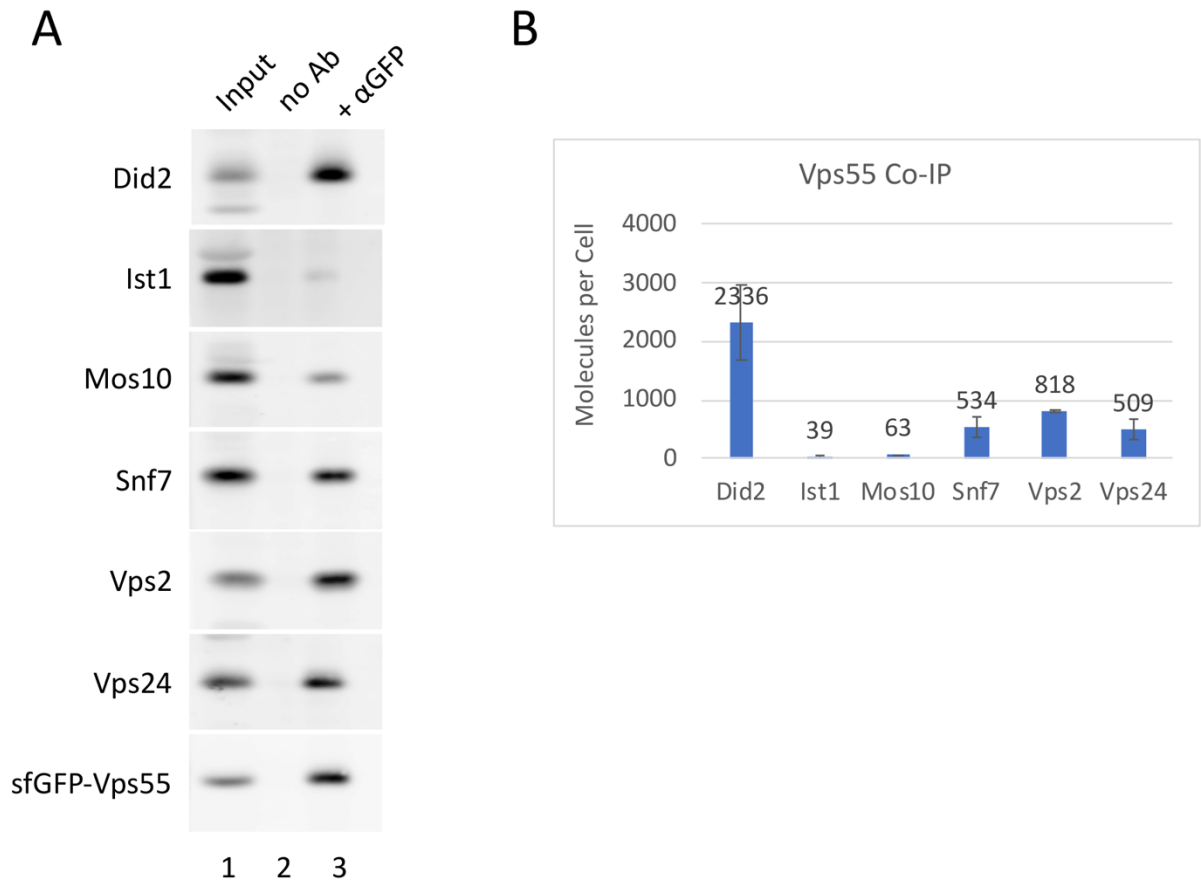

Figure 1: Vps55 interacts with ESCRT-III. sfGFP-Vps55 was immunoprecipitated from cell extracts of RKY3427 with anti-GFP antibodies. (A) The immunoprecipitates were analyzed for the presence of ESCRT-III proteins by western blotting with specific antibodies against the different ESCRT-III proteins as indicated. Lane 1: input, lane 2: IP without GFP antibodies, lane 3: IP with GFP antibodies (primary IP, bottom panel: 20 % of input, co-IP, top panels: 2 % of input). (B) The western blot signals were quantified with ImageJ and it was calculated (as described previously) (Heinzle et al., 2019) how many molecules of each ESCRT-III protein are present in complexes per cell.

For detection Vps55 was tagged with superfolder GFP at its N-terminus (sfGFP-Vps55). Vps55 was immunoprecipitated from cell extracts with anti-sfGFP antibodies and the immunoprecipitates were analyzed for the presence of ESCRT-III proteins by western blotting (Fig. 1A). All tested ESCRT-III proteins could be specifically co-immunoprecipitated with sfGFP-Vps55. From the co-IP signals it was calculated how many molecules of each ESCRT-III protein are present in ESCRT-III complexes per cell (as described previously) (Heinzle et al., 2019) (Fig. 1B). The co-IP pattern was in line with our previous observations. Did2 turned out to be the most abundant ESCRT-III protein with about 2000 molecules in the complexes, while the core ESCRT-III components Snf7, Vps2 and Vps24 were present in about equimolar amounts with about 500-800 molecules. In addition, a small number of Ist1 and Mos10 molecules was detected in the complexes. Interestingly, in co-IP experiments with individual ESCRT-III subunits about the same numbers were obtained (Heinzle et al., 2019). This suggests that probably all ESCRT-III complexes in the cell are associated with Vps55. Thus, Vps55 behaves like a subunit of ESCRT-III

Kinetics of Ste6 turnover in the VPS68 deletion mutant

The short-lived endocytic cargo protein Ste6 is transported to the yeast vacuole for degradation via the multivesicular body pathway (Kölling and Hollenberg, 1994). As described before, Ste6 is stabilized in the *Δvps68* mutant (Alsleben and Kölling, 2022). We now took a closer look at the kinetics of Ste6 degradation using a gal-depletion experiment. Cells containing *STE6* under the control of the *GAL1* promoter were grown on galactose containing medium to induce expression of *STE6* and were then shifted to glucose containing medium to repress expression from the *GAL1* promoter. Then equal aliquots of cells were collected at time intervals and examined for the amount of Ste6 present (Fig. 2). In general, Ste6 degradation follows first order kinetics, i.e. the amount of Ste6 degraded per time only depends on the total amount of Ste6 present. This behavior was observed with the wildtype strain (Fig. 2) as well as with many mutants in the vacuolar protein sorting (vps) pathway in previous experiments. But in the case of *Δvps68* an unusual time course was observed. During the first 20 min the protein was barely degraded, but thereafter degradation occurred with a near wildtype rate. This unusual profile is not related to problems in glucose repression, since the same behavior was seen in cycloheximide chase experiments, where expression is blocked on a translational level (not shown). Also, similar degradation profiles were reported in another study with pulse-chase experiments for the a-factor receptor Ste3 in *Δvps55* and *Δvps68* mutants (Schluter et al., 2008). Thus, it appears that a certain process, which occurs before degradation of Ste6 is initiated, is slowed down in the *Δvps68* mutant.

To substantiate this notion, we tried to set up a simple model, which recapitulates the experimentally observed shape of the degradation curve (Fig. 2D, E). We made the following assumptions: i) degradation of Ste6 is delayed by 20 min, ii) during this time Ste6 is converted to a degradation competent form, iii) the conversion rate is non-linear and increases exponentially over time (with this assumption the best fit was obtained). When the *STE6* expression is turned off, the total Ste6 pool consists of a mixture of states depending on how

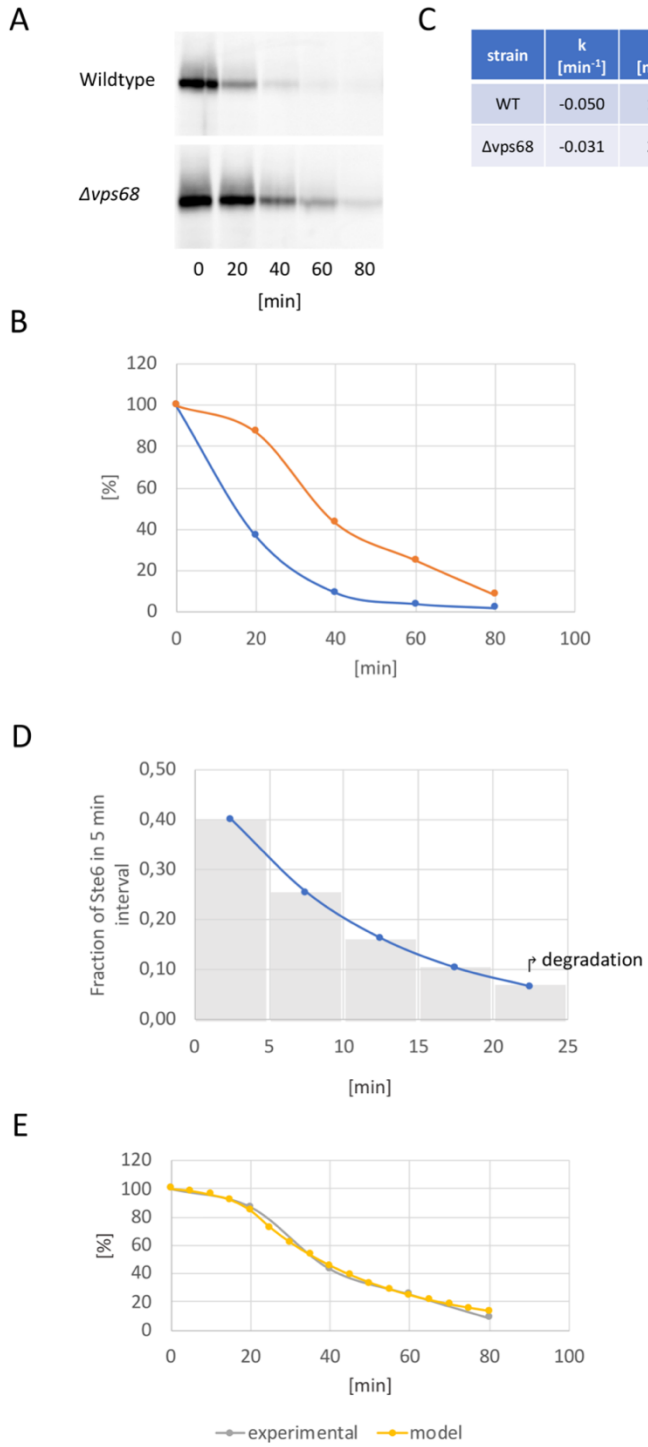

strain	k [min^{-1}]	τ [min]	R^2
WT	-0.050	14	0.998
Δvps68	-0.031	22	0.880

Figure 2: Kinetics of Ste6 degradation in the *Δvps68* mutant. The Ste6 turnover was investigated by a gal depletion experiment. (A) Equal aliquots of cell culture were collected at different time points after *GAL1* promoter shut-off (t_0) and examined for Ste6 by western blotting. Top panel: RKY3319 (wildtype), bottom panel: RKY3320 (*Δvps68*). (B) The western blot signals were quantified by ImageJ. (C) The rate constant (k), the half-life (τ) and the correlation coefficient (R^2) were calculated for the two strains from the data in (B). (D) Model for the distribution of Ste6 to different maturation states at time t_0. According to the model it takes 20 min before Ste6 degradation starts. The maturation time is shown on the x-axis, degradation starts after the protein has spent 20 min in the maturation compartment. (E) Comparison of the experimental data with the data predicted by the model.

far the conversion to the degradation competent form has progressed. To incorporate this into our model and for a simple numerical solution of the problem, the maturation period was divided into five segments and the Ste6 protein was allocated to these five segments based on the assumption that the conversion rate increases over time. This results in the Ste6 distribution depicted in Fig. 2D. Degradation of Ste6 in the different segments then starts after a delay of 0, 5, 10, 15 or 20 min depending on its location in the maturation pathway after *GAL1* promoter shut-off. For the calculations the rate constant determined in Fig. 2B was used (k= -0.031 min^{-1}). With these assumptions a perfect fit between the model and the experimental data was achieved (Fig. 2E). From this we conclude that Vps68 plays a role in converting Ste6 to a degradation competent form and that this process is extended to 20 min, when Vps68 is not present. It is reasonable to assume that the process, which is slowed down in *Δvps68*, is the formation of intraluminal vesicles during MVB formation.

A

Interactor	Correlation
VPS55	0.64428
DID2	0.54139
ATG21	0.54031
MSP1	0.51866
TMS1	0.51702
MVB12	0.51664
HST2	0.51262

B

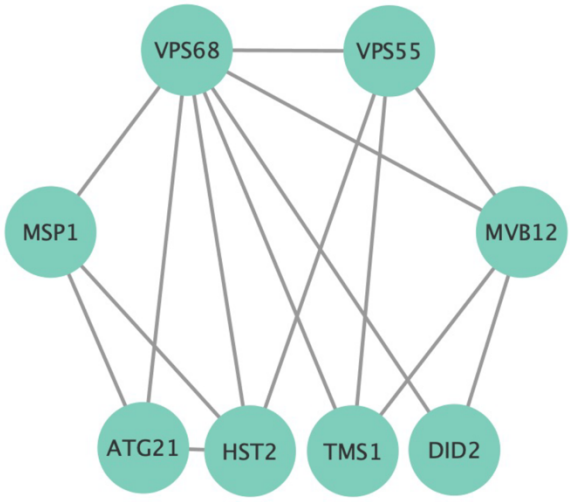

C

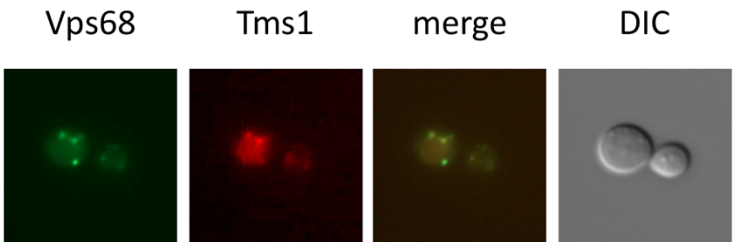

Figure 3: Co-fitness interactions between the *VPS68* deletion and other deletion mutants. (A) The top scoring interactors with the *VPS68* deletion obtained from the Yeast Fitness Database (Hillenmeyer et al., 2010). Listed are the deletion mutants with a co-fitness score above 0.5. (B) Co-fitness interactions with a co-fitness score of at least 0.4 among the top scoring interactors of *Δvps68*. (C) Tms1 co-localizes with Vps68. The localization of sfGFP-Vps68 and Tms1-mCherry in strain RKY3653 was examined by fluorescence microscopy.

Parallel function of the Vps55/Vps68 complex and the SERINC homologue Tms1

To identify proteins that are functionally related to Vps55/Vps68 we consulted the "Yeast Fitness Database" (Hillenmeyer et al., 2010). There the growth fitness of deletion strains from the yeast whole-genome deletion collection in the presence of various chemicals was quantified. For each pair of deletions, the fitness profiles across all experiments were compared and a co-fitness score was calculated, which varies between -1 (no correlation at all, opposite phenotype) and +1 (perfect correlation, identical phenotype). The seven top scoring interactors for *VPS68* (correlation >0.5) are listed in Fig. 3A (description of the genes in Tab.S2). The validity of the dataset is underscored by the finding that the *VPS55* deletion was the top scoring interaction (correlation=0.644). Second on the list of top scoring interactors is the ESCRT-III protein Did2, which could be involved in the Vps55/Vps68/ESCRT-III interaction. Another ESCRT-protein on the list is Mvb12, a member of ESCRT-I. We also examined the top scoring deletions for co-fitness among each other. Intriguingly, the deletions form a highly interconnected network of co-fitness interactions (Fig. 3B).

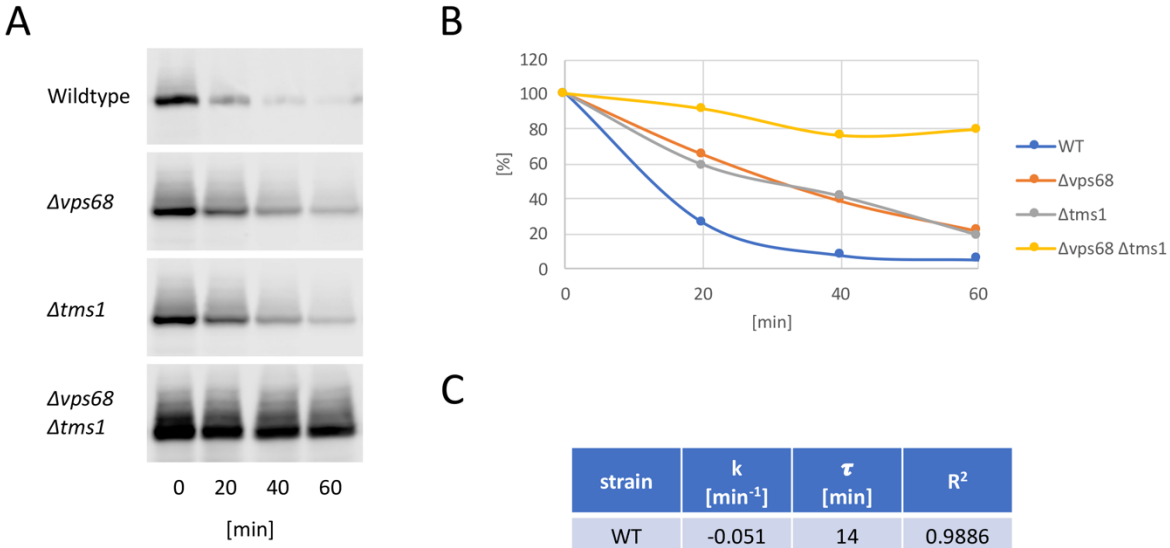

strain	k [min^{-1}]	τ [min]	R^2
WT	-0.051	14	0.9886
Δvps68	-0.026	27	0.9946
Δtms1	-0.027	26	0.9895
Δvps68 Δtms1	-0.004	173	0.8304

Figure 4: Ste6 is strongly stabilized in a *Δtms1 Δvps68* double mutant. The Ste6 turnover was investigated by a gal depletion experiment. (A) Equal aliquots of cell culture were collected at time intervals and examined for Ste6 by western blotting. Different from the experiment in Fig. 2, the collection of samples was started 20 min after *GAL1* promoter shut-off. From top to bottom: RKY3319 (WT), RKY3320 (*Δvps68*}, RKY3659 (*Δtms1*}, RKY3660 (*Δtms1 Δvps68*). (B) The western blot signals were quantified by ImageJ. (C) The rate constant (k), the half-life (τ) and the correlation coefficient (R^2) were calculated for the strains from the data in (B).

The SERINC homologue Tms1 was selected for further study, since it bears some resemblance with the Vps55/Vps68 complex (Fig. S1). The core structure of the SERINC protein family is formed by two blocks of four transmembrane domains (TMDs) (Leonhardt et al., 2023; Pye et

al., 2020) and Vps55 and Vps68 consist of four putative TMDs each. So far, no phenotype could be detected for the *TMS1* deletion (Grossman et al., 2000). First the intracellular localization of Tms1 was examined by fluorescence microscopy with gene fusions integrated into the yeast genome. With Tms1-mCherry about half a dozen dots were observed, which perfectly colocalized with sfGFP-Vps68 dots (Fig. 3C). This indicates that Vps55/Vps68 and Tms1 function at the same site in the cell. The dots most likely correspond to endosomal structures.

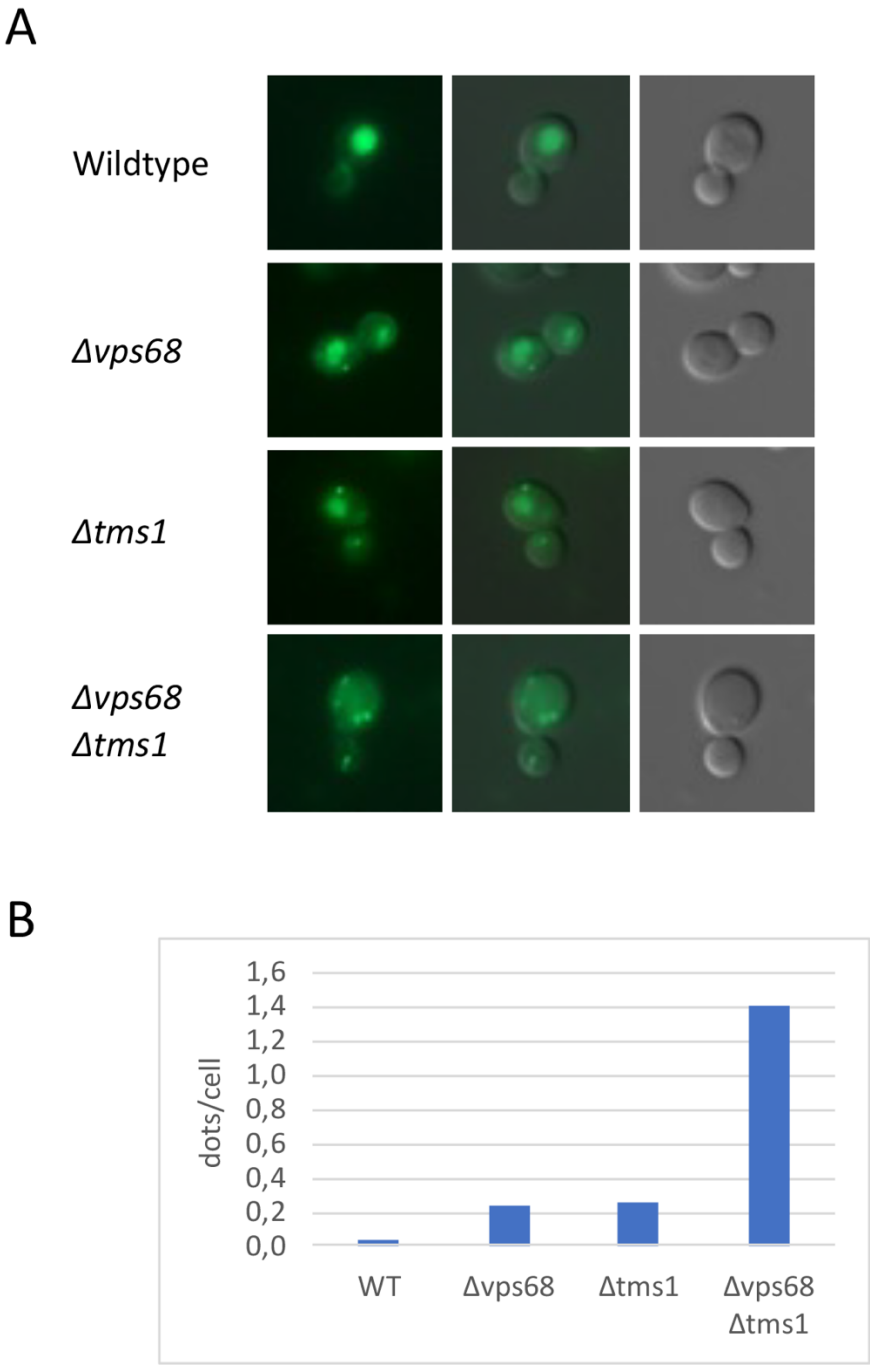

Figure 5: Effect of *TMS1* and *VPS68* deletions on the intracellular localization of Ste6. (A) The localization of Ste6-GFP expressed from the single copy plasmid pRK744 was examined in the different mutant strains by fluorescence microscopy. From top to bottom: RKY3319 (WT), RKY3320 (*Δvps68*}, RKY3659 (*Δtms1*), RKY3660 (*Δtms1 Δvps68*). (B) Quantification of the number of endosomal dots per cell.

To see whether Tms1 is involved in endocytic trafficking like Vps55/Vps68, we examined its role in Ste6 degradation by a gal-depletion experiment (Fig. 4). The *TMS1* deletion displayed the same degree of stabilization as the *VPS68* deletion (half-lives 26 min and 27 min, respectively, compared to 14 min for the wildtype). Thus, both deletions moderately affect the half-life of Ste6 in a similar manner. However, when both deletions were combined, the Ste6 protein was completely stable (half-life 173 min). This pronounced synthetic phenotype indicates that the Vps55/Vps68 complex and Tms1 perform the same, parallel function at endosomes.

Next, the effect of the *VPS68* and *TMS1* deletions on the intracellular localization of Ste6-GFP was examined (Fig. 5). In the wildtype strain GFP staining was mostly detected in the lumen of the vacuole, reflecting the high constitutive turnover of Ste6. Occasionally, a dot-like structure was observed next to the vacuole (0.04 dots/cell). In the *Δvps68* and *Δtms1* single mutants basically the same pattern was seen, but with a higher number of dots (0.24 and 0.26 dots/cell). In the double mutant the number of dots was increased to 1.4 dots/cell. This localization pattern is different from the ones previously described for other vacuolar protein sorting (*vps*) mutants (Raymond et al., 1992). According to this classification, Ste6-GFP neither displays a class D nor a class E localization. In class D mutants Ste6 shows enhanced recycling to the bud cell surface (Krsmanovic´ et al., 2005) and in class E mutants it accumulates in a brightly staining dot next to the vacuole and in the limiting membrane of the vacuole (Kranz et al., 2001). In the *Δvps68 Δtms1* mutant just the number of late endosomes appears to be increased.

In conclusion, our data establish a link between lipid remodeling and ESCRT-III function. The Vps55/Vps68 complex appears to perform the same or a similar function as the SERINC homologue Tms1. Since human SERINCs are lipid-flipping scramblases, it is likely that Vps55/Vps68 has a similar activity. Loss of this activity leads to a delay in the degradation of the endocytic cargo protein Ste6. Since Vps55/Vps68 directly associates with ESCRT-III, it is plausible to assume that lipid remodeling at the site of ILV formation is crucial for ESCRT-III function.

Materials and methods

Yeast strains and media

For immunoprecipitation experiments yeast cells were grown overnight to exponential phase in YPD medium (1 % yeast extract, 2 % peptone, 2 % glucose), for gal depletion experiments they were first grown overnight to exponential phase in YPGal medium (1 % yeast extract, 2 % peptone, 2 % galactose, 0.2 % glucose) and were then shifted to YPD medium. For fluorescence microscopy cells were grown in SD/CAS medium (0.67 % yeast nitrogen base, 1 % casamino acids, 2 % glucose, 50 mg/l uracil and tryptophan) to avoid autofluorescence from the YPD medium. For plasmid selection uracil was omitted from the medium. The yeast strains used are listed in Tab. S1. All yeast strains are derived from JD52 (J. Dohmen, Cologne, Germany) by the integration of PCR-cassettes into the yeast genome (Longtine et al., 1998).

Plasmid pRK744 is a CEN plasmid with URA3 marker carrying a *STE6-GFP* fusion under the control of the *STE6* promoter.

Co-immunoprecipitation

For Co-immunoprecipitation (Co-IP) experiments, 50 OD_{600} cells of an exponential YPD culture were harvested, washed with PBS and resuspended in 200 µl PBS with protease inhibitors. The cells were lysed by glass-beading for 5 min at 4°C. After lysis, 600 µl PBS were added and the solution was spun at 500 g for 5 min to remove cell debris. Then 2.5 mM of the cleavable crosslinker DSP (dithiobis (succinimidylpropionate)) (Thermo Scientific, Waltham, USA) were added to the supernatant and the solution was incubated for 30 min at RT on a rocker. The crosslinking reaction was stopped by quenching with 100 mM Tris-HCl pH 8.0 and the membranes were dissolved by 1 % Triton X-100 for 15 min at RT on a rocker. Another 500 g spin was applied to remove any formed precipitates. Then the supernatant was incubated with anti-GFP antibodies (Nordic-MUbio, Susteren, Netherlands) for 1 h at 4°C on a rocker followed by an incubation with 200 µl of a 20 % slurry of protein A sepharose beads (GE Healthcare, Uppsala, Sweden) for 1 h at 4°C. The solution was washed three times with 1 ml PBS at 500 g for 1 min. The beads were resuspended in a mixture of 100 µl PBS and 100 µl SDS sample buffer and heated to 95°C for 5 min. Then the immunoprecipitates were analyzed for the presence of ESCRT-III proteins by western blotting with specific antibodies.

Fluorescence microscopy

Yeast cells were grown overnight to exponential phase in SD/CAS medium. The yeast cell suspension was applied to concanavalin A coated slides and imaged with a Zeiss Axio-Imager M1 fluorescence microscope equipped with an AxioCam MRm camera (Zeiss, Göttingen, Germany). Images were acquired with the Axiovision Software and processed with Photoshop Elements.

References

Alli-Balogun, G.O., and T.P. Levine. 2021. Fungal Ice2p is in the same superfamily as SERINCs, restriction factors for HIV and other viruses. *Proteins*. 89:1240-1250.

Alsleben, S., and R. Kölling. 2022. Vps68 cooperates with ESCRT-III in intraluminal vesicle formation. *J Cell Sci*. 135.

Azmi, I.F., B.A. Davies, J. Xiao, M. Babst, Z. Xu, and D.J. Katzmann. 2008. ESCRT-III family members stimulate Vps4 ATPase activity directly or via Vta1. *Dev Cell*. 14:50-61.

Babst, M., D.J. Katzmann, E.J. Estepa-Sabal, T. Meerloo, and S.D. Emr. 2002. ESCRT-III: an endosome-associated heterooligomeric protein complex required for MVB sorting. *Dev Cell*. 3:271-282.

Belgareh-Touze, N., S. Avaro, Y. Rouille, B. Hoflack, and R. Haguenauer-Tsapis. 2002. Yeast Vps55p, a functional homolog of human obesity receptor gene-related protein, is involved in late endosome to vacuole trafficking. *Mol Biol Cell*. 13:1694-1708.

Gatta, A.T., and J.G. Carlton. 2019. The ESCRT-machinery: closing holes and expanding roles. *Curr Opin Cell Biol*. 59:121-132.

Grossman, T.R., J.M. Luque, and N. Nelson. 2000. Identification of a ubiquitous family of membrane proteins and their expression in mouse brain. *J Exp Biol*. 203:447-457.

Heinzle, C., L. Mücke, T. Brune, and R. Kölling. 2019. Comprehensive analysis of yeast ESCRT-III composition in single ESCRT-III deletion mutants. *Biochem J*. 476:2031-2046.

Henne, W.M., H. Stenmark, and S.D. Emr. 2013. Molecular mechanisms of the membrane sculpting ESCRT pathway. *Cold Spring Harb Perspect Biol*. 5.

Hillenmeyer, M.E., E. Ericson, R.W. Davis, C. Nislow, D. Koller, and G. Giaever. 2010. Systematic analysis of genome-wide fitness data in yeast reveals novel gene function and drug action. *Genome Biol*. 11:R30.

Huh, W.K., J.V. Falvo, L.C. Gerke, A.S. Carroll, R.W. Howson, J.S. Weissman, and E.K. O'Shea. 2003. Global analysis of protein localization in budding yeast. *Nature*. 425:686-691.

Inuzuka, M., M. Hayakawa, and T. Ingi. 2005. Serinc, an activity-regulated protein family, incorporates serine into membrane lipid synthesis. *J Biol Chem*. 280:35776-35783.

Kölling, R., and C.P. Hollenberg. 1994. The ABC-transporter Ste6 accumulates in the plasma membrane in a ubiquitinated form in endocytosis mutants. *EMBO J.* 13:3261-3271.

Kranz, A., A. Kinner, and R. Kölling. 2001. A family of small coiled-coil-forming proteins functioning at the late endosome in yeast. *Mol Biol Cell*. 12:711-723.

Krsmanovic´, T., A. Pavelec, T. Sydor, and R. Kölling. 2005. Control of Ste6 recycling in the early endocytic pathway in yeast. *Mol. Biol. Cell*. 16:2809-2821.

Leonhardt, S.A., M.D. Purdy, J.R. Grover, Z. Yang, S. Poulos, W.E. McIntire, E.A. Tatham, S.K. Erramilli, K. Nosol, K.K. Lai, S. Ding, M. Lu, P.D. Uchil, A. Finzi, A. Rein, A.A. Kossiakoff, W. Mothes, and M. Yeager. 2023. Antiviral HIV-1 SERINC restriction factors disrupt virus membrane asymmetry. *Nat Commun*. 14:4368.

Longtine, M.S., A. McKenzie, D.J. Demarini, N.G. Shah, A. Wach, A. Brachat, P. Philippsen, and J.R. Pringle. 1998. Additional modules for versatile and economical PCR-based gene deletion and modification in *Saccharomyces cerevisiae*. *Yeast*. 14:953-961.

Matsuo, H., J. Chevallier, N. Mayran, I. Le Blanc, C. Ferguson, J. Faure, N.S. Blanc, S. Matile, J. Dubochet, R. Sadoul, R.G. Parton, F. Vilbois, and J. Gruenberg. 2004. Role of LBPA and Alix in multivesicular liposome formation and endosome organization. *Science*. 303:531-534.

Nickerson, D.P., M. West, and G. Odorizzi. 2006. Did2 coordinates Vps4-mediated dissociation of ESCRT-III from endosomes. *J Cell Biol*. 175:715-720.

Pfitzner, A.K., J. Moser von Filseck, and A. Roux. 2021. Principles of membrane remodeling by dynamic ESCRT-III polymers. *Trends Cell Biol*. 31:856-868.

Pfitzner, A.K., H. Zivkovic, C. Bernat-Silvestre, M. West, T. Peltier, F. Humbert, G. Odorizzi, and A. Roux. 2023. Vps60 initiates alternative ESCRT-III filaments. *J Cell Biol*. 222.

Pye, V.E., A. Rosa, C. Bertelli, W.B. Struwe, S.L. Maslen, R. Corey, I. Liko, M. Hassall, G. Mattiuzzo, A. Ballandras-Colas, A. Nans, Y. Takeuchi, P.J. Stansfeld, J.M. Skehel, C.V. Robinson, M. Pizzato, and P. Cherepanov. 2020. A bipartite structural organization defines the SERINC family of HIV-1 restriction factors. *Nat Struct Mol Biol*. 27:78-83.

Raymond, C.K., S.I. Howald, C.A. Vater, and T.H. Stevens. 1992. Morphological classification of the yeast vacuolar protein sorting mutants: evidence for a prevacuolar compartment in class E *vps* mutants. *Mol Biol Cell*. 3:1389-1402.

Remec Pavlin, M., and J.H. Hurley. 2020. The ESCRTs - converging on mechanism. *J Cell Sci*. 133.

Rosa, A., A. Chande, S. Ziglio, V. De Sanctis, R. Bertorelli, S.L. Goh, S.M. McCauley, A. Nowosielska, S.E. Antonarakis, J. Luban, F.A. Santoni, and M. Pizzato. 2015. HIV-1 Nef promotes infection by excluding SERINC5 from virion incorporation. *Nature*. 526:212-217.

Rue, S.M., S. Mattei, S. Saksena, and S.D. Emr. 2008. Novel Ist1-Did2 complex functions at a late step in multivesicular body sorting. *Mol Biol Cell*. 19:475-484.

Schluter, C., K.K. Lam, J. Brumm, B.W. Wu, M. Saunders, T.H. Stevens, J. Bryan, and E. Conibear. 2008. Global analysis of yeast endosomal transport identifies the vps55/68 sorting complex. *Mol Biol Cell*. 19:1282-1294.

Suzuki, S.W., A. Oishi, N. Nikulin, J.R. Jorgensen, M.G. Baile, and S.D. Emr. 2021. A PX-BAR protein Mvp1/SNX8 and a dynamin-like GTPase Vps1 drive endosomal recycling. *Elife*. 10.

Trautz, B., H. Wiedemann, C. Luchtenborg, V. Pierini, J. Kranich, B. Glass, H.G. Krausslich, T. Brocker, M. Pizzato, A. Ruggieri, B. Brugger, and O.T. Fackler. 2017. The host-cell restriction factor SERINC5 restricts HIV-1 infectivity without altering the lipid composition and organization of viral particles. *J Biol Chem*. 292:13702-13713.

Usami, Y., Y. Wu, and H.G. Gottlinger. 2015. SERINC3 and SERINC5 restrict HIV-1 infectivity and are counteracted by Nef. *Nature*. 526:218-223.

Varadi, M., S. Anyango, M. Deshpande, S. Nair, C. Natassia, G. Yordanova, D. Yuan, O. Stroe, G. Wood, A. Laydon, A. Zidek, T. Green, K. Tunyasuvunakool, S. Petersen, J. Jumper, E. Clancy, R. Green, A. Vora, M. Lutfi, M. Figurnov, A. Cowie, N. Hobbs, P. Kohli, G. Kleywegt, E. Birney, D. Hassabis, and S. Velankar. 2022. AlphaFold Protein Structure Database: massively expanding the structural coverage of protein-sequence space with high-accuracy models. *Nucleic Acids Res*. 50:D439-D444.

Vietri, M., M. Radulovic, and H. Stenmark. 2020. The many functions of ESCRTs. *Nat Rev Mol Cell Biol*. 21:25-42.

Data availability

All data are available in the main text or supplementary materials.

Acknowlegdements

I like to thank Thomas Brune for his assistance with the experiments.

Author contributions

The study was conceived, conducted and written by R. Kölling.

Supplemental material

Tab S1: Yeast strains

Strain	Genotype	
JD52	*MATa ura3-52 his3-Δ200 leu2-3,112 trp1-Δ63 lys2-801 ssd1-d2*	J. Dohmen, Köln
RKY3319	*ste6::[kan GAL1p-STE6]*	this study
RKY3320	*ste6::[His3 GAL1p-STE6] Δvps68::kan*	this study
RKY3427	*vps55::[kan SNF7p-sfGFP-VPS55]*	this study
RKY3653	*TMS1-mCherry::His3 vps68::[kan SNF7p-sfGFP-VPS68]*	this study
RKY3659	*ste6::[kan GAL1p-STE6] Δtms1::TRP1*	this study
RKY3660	*ste6::[His3 GAL1p-STE6] Δtms1::TRP1 Δvps68::kan*	this study

Tab. S2: *Saccharomyces* Genome Database (SGD) descriptions of interactors

Gene	**Description**
ATG21	Phosphoinositide binding protein; required for vesicle formation in cytoplasm-to-vacuole targeting (CVT) pathway, autophagy, micronucleophagy and mitophagy; binds to several phosphoinositides including PtdIns(3,5)P2, PI3P and PI4P; involved in PI3P-dependent recruitment and organization of both Atg12-Atg5-Atg16 complex and Atg8p at pre-autophagosomal structure; necessary for oxidant-induced cell death; targeted to vacuole via AP-3 pathway; WD-40 repeat containing PROPPIN family member
DID2	Class E protein of the vacuolar protein-sorting (Vps) pathway; binds Vps4p and directs it to dissociate ESCRT-III complexes; forms a functional and physical complex with Ist1p; human ortholog may be altered in breast tumors
HST2	Cytoplasmic NAD(+)-dependent protein deacetylase; deacetylation targets are primarily cytoplasmic proteins; member of the silencing information regulator 2 (Sir2) family of NAD(+)-dependent protein deacetylases; modulates nucleolar (rDNA) and telomeric silencing; possesses NAD(+)-dependent histone deacetylase activity in vitro; contains a nuclear export signal (NES); function regulated by its nuclear export
MSP1	Highly-conserved N-terminally anchored AAA-ATPase; distributed in the mitochondrial outer membrane and peroxisomes; involved in mitochondrial protein sorting; functions as an extraction engine in local organelle surveillance to remove and initiate degradation of mistargeted proteins, ensuring fidelity of organelle-specific localization of tail-anchored proteins; contains an N-terminal transmembrane domain and C-terminal cytoplasmic ATPase domain
MVB12	ESCRT-I subunit required to stabilize ESCRT-I core complex oligomers; the ESCRT-I core complex (Stp22p, Vps28p, Srn2p) is involved in ubiquitin-dependent sorting of proteins into the endosome; deletion mutant is sensitive to rapamycin and nystatin
TMS1	Vacuolar membrane protein of unknown function; is conserved in mammals; predicted to contain eleven transmembrane helices; interacts with Pdr5p, a protein involved in multidrug resistance
VPS55	Late endosomal protein involved in late endosome to vacuole transport; functional homolog of human obesity receptor gene-related protein (OB-RGRP)

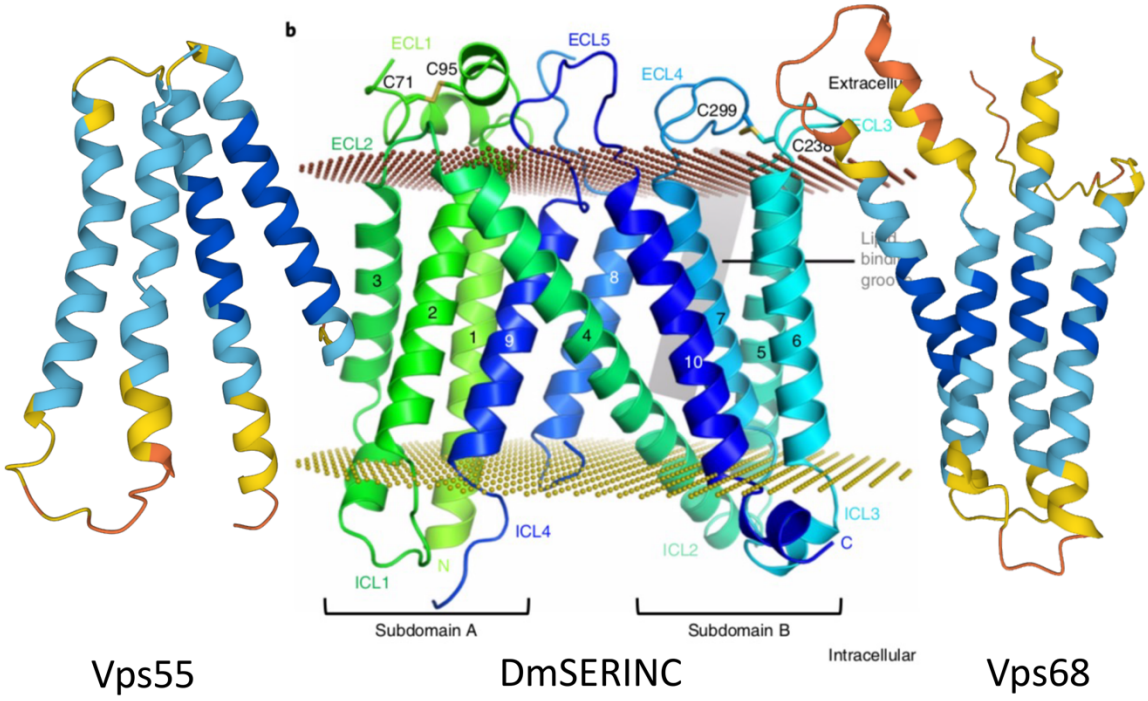

Figure S1: The cryo-EM structure of DmSERINC taken from (Pye et al., 2020) is compared with the structures of Vps55 and Vps68 as predicted by AlphaFold (Varadi et al., 2022).